Phase Behavior of Aqueous Solutions of Hydroxypropylcellulose

Stefano Guido

Dipartimento di Ingegneria Chimica, Università di Napoli "Federico II", 80125 Napoli, Italy

Received January 23, 1995; Revised Manuscript Received April 5, 1995[⊗]

ABSTRACT: The phase behavior of hydroxypropylcellulose (HPC) in water has been studied in the temperature range from −3 to +46 °C by video-enhanced contrast (VEC) optical microscopy. In the low temperature range (below about 18 °C), a significant thermotropic effect was found in a narrow biphasic gap, with the critical HPC concentration for mesophase formation rapidly increasing as a function of temperature. The effect can be explained in terms of an increase of chain rigidity upon lowering the temperature, as estimated from intrinsic viscosity measurements. At higher temperatures (up to about 40 °C), phase separation takes place in a wider region, which extends to a polymer concentration of about 65% wt at 25 °C. Upon a further increase in temperature, the material becomes white and turbid in a broad concentration range. When samples are examined at high magnification with the VEC optics, three distinct morphologies are observed in the turbid region, depending on concentration. At low concentrations, anisotropic spherulites are dispersed in an anisotropic medium. At high concentrations, isotropic inclusions of irregular shape are observed in an anisotropic continuous phase. A gel-like structure, characterized by a three-dimensional network, is displayed by solutions of intermediate concentrations. The phase diagram here obtained is compared to previous results on the HPC/water system and discussed in terms of the existing theories on liquid crystalline polymer thermodynamics.

1. Introduction

Hydroxypropylcellulose (HPC) is a water soluble ether of native cellulose.[1] Concentrated aqueous solutions of HPC display optical properties typical of cholesteric liquid crystals,[2] such as selective reflection in the visible region of the spectrum (which gives rise to intense iridescent colors), a peculiar optical rotary dispersion curve, and a ringed light diffraction pattern.[3] Such properties are a consequence of the cholesteric layered arrangement of the polymer chains.[4] When the helical axis is viewed from the side, a set of equidistant dark lines, corresponding to layers with orientation parallel to the direction of observation, can be seen (the so-called fingerprint texture). The spacing between the fingerprint lines is equal to half the helical pitch P.[4] The diffraction ring, for example, can be explained by regarding the fingerprint texture as a two-dimensional phase grating or, alternatively, by considering Bragg-like reflections from the cholesteric planes.[3]

While typical cholesteric structures, including the fingerprint lines, have been documented by light microscopy for HPC in acetic acid,[3,5] pyridine,[6] and methoxyethanol,[6] the helical pitch for HPC in water has been considered not resolvable by several authors.[3,5] Only recently has the use of video-enhanced contrast (VEC) optical microscopy allowed a direct visualization of the fingerprint lines, which were resolved up to a HPC concentration of about 50% wt (corresponding to a spacing of 0.4 μm).[7] This result proposes VEC microscopy as a valuable tool to study the phase behavior of HPC in water. Indeed, the anisotropic region of the phase diagram can be determined by imaging the cholesteric textures displayed in the liquid crystalline state (such as the fingerprint lines), without resorting to indirect methods. For most lyotropic liquid crystal polymers (LCP), the pitch of the helical structure in a given solvent is a decreasing function of concentration.[8] At high concentrations (above ca. 50% wt), even though the fingerprint lines are no longer resolvable in optical microscopy, the VEC technique can still be applied to distinguish anisotropic solutions, since typical cholesteric textures, such as planar configurations and polygonal fields, can be clearly observed between crossed polars.[7]

So far, the phase behavior of HPC in water has been investigated by several experimental methods, including turbidimetry, hot stage optical microscopy, ultracentrifugation, viscosimetry, differential scanning calorimetry, light and X-ray scattering, nuclear magnetic resonance, and analytical techniques.[5,9−18] At room temperature, the critical concentration for mesophase formation, which is a fundamental quantity for comparison with theories, was found to be substantially independent of molecular weight. Literature values are in the range 36−42% wt, corresponding to volume fractions v'_2 from 0.32 to 0.39,[5,9,11,14,16,17,19] as shown in Table 1. Furthermore, v'_2 and v''_2 have been reported to be independent of temperature in the range 0−25 °C.[11] Literature values for the upper limit of the biphasic region v''_2 range from 0.42 to 0.51 (see Table 1).

An accurate determination of the width of the biphasic region is not just important for comparison with existing theories (the relevant quantity is the ratio v''_2/v'_2, which is also predicted to depend on sample polydispersity[20]). Since HPC in water is widely used as a model system for rheo-optical studies on liquid crystalline behavior in polymers, it is essential to know the range of temperature and concentration where the solutions are fully anisotropic. So far, samples with concentrations ranging from 50% to 60% wt have been considered as fully liquid crystalline at room temperature. However, it has been recently shown that commercial HPC solutions are still biphasic at 60% wt and that phase separation has both qualitative and quantitative effects on the rheological response of the HPC/water system.[21] A more detailed investigation of the biphasic region appears, therefore, in order.

Another feature characteristic of the phase behavior of HPC in water is the steep increase in turbidity upon heating above ca. 40 °C,[16] suggesting the occurrence of phase separation. The exact value of the transition temperature depends on concentration. Good agreement on cloud point determination is found in the

[⊗] Abstract published in *Advance ACS Abstracts,* June 1, 1995.

0024-9297/95/2228-4530$09.00/0

Table 1

HPC source	M_w (M_w/M_n)	MS[b]	v'_2	v''_2	v''_2/v'_2	T, °C	ref
Hercules, Klucel L	100 000[a]	3	0.39	0.51	1.31	25	17
Hercules, Klucel EF[c]	30 000	3	0.37			20	9
Hercules, Klucel EF	132 000	3	0.35			20	9
Hercules, Klucel LF	150 400	3	0.34	0.42	1.23	20	9
Hercules, Klucel GF	479 000	3	0.32			20	9
Aldrich[c]	28 000 (2.0)	6.3		~0.50		15	11
Aldrich[c]	140 000 (1.8)	5.8		~0.50		25	11
Aldrich	100 000[a]		0.36	0.42	1.17	room	7
Hercules, Klucel L	140 000		0.38	0.45	1.18	23	14
Tokyo Kasei Kogyo Co.	93 000	4.2	0.39			25	19
Hercules, Klucel E	60 000[a]		0.37			room	16
Hercules, Klucel L	100 000[a]		0.38			room	16
Hercules, Klucel H	1 000 000[a]		0.35			room	16

[a] Nominal value. [b] Molar substitution (see Materials and Methods). [c] Fraction.

literature for dilute solutions, whereas values as different as 36[22] and 65 °C[23] have been reported for a 60% wt sample. Furthermore, the nature of the phases at equilibrium above the transition temperature is not known with certainty, the occurrence of a gel state being proposed by several authors.[9,16,18,23] Phase separation has been described in terms of a lower critical solution temperature (LCST),[18,24] but even though HPC solubility in water increases with decreasing temperature,[25] there is no clear minimum or critical point.

In this work, the phase diagram of aqueous solutions of commercial HPC has been studied by VEC microscopy. The high-magnification VEC system used in this work generates high-quality images of structural features close to the theoretical limit of resolution for the optical microscope, thus allowing one to observe the texture of the phases at equilibrium throughout the temperature range investigated. Two issues have been specifically addressed, namely, (i) the temperature dependence of the limits of the narrow biphasic region and (ii) the nature of the turbid state occurring above ca. 40 °C. The results of (i) have been compared with measurements of intrinsic viscosity as a function of temperature. The dependence of the helical pitch on concentration and temperature has also been studied.

2. Experimental Section

2.1. Materials. HPC (Klucel E and EF) was supplied by Aqualon. The molecular weight of HPC–EF was estimated from the intrinsic viscosity at 25 °C in water, using the following relationships given by Wirick and Waldman[1]

$$[\eta] = 2.6 \times 10^5 M_w^{0.9} \quad (1a)$$

$$[\eta] = 7.2 \times 10^{-3} DP_w^{0.915} \quad (1b)$$

where DP_w is the weight average degree of polymerization. Equation 1a provides only a rough estimate of M_w (ca. 127 000), given the difference in molar substitution MS (the average number of moles of hydroxypropyl substituent per mole of anhydroglucose residue) between the sample used in this work (MS = 3.7 according to the manufacturer) and the ones characterized by Wirick and Waldman (MS between 4 and 5). A better estimate is obtained by using eq 1b. Indeed, since MS decreases slightly with increasing M_w,[26] eq 1b allows one to account for such an effect. In particular, since the molecular weight of the anhydroglucose unit corresponding to MS = 3.7 is 376, a value of M_w = 85 000 can be derived from eq 1b, much closer to the nominal value (80 000).

The intrinsic viscosity was measured as a function of temperature in the range 1–35°C by using Cannon-Ubbelhode viscometers. At low temperatures, the flow times were observed to decrease in the course of time (the higher the dilution, the more marked the decrease, up to about 1%). A similar effect has been reported for HPC in DCA and attributed to polymer degradation.[27] Measurements were therefore repeated until the variation in flow time was within experimental error. More details on the calculation of $[\eta]$ will be given in the Results.

HPC samples were dried under vacuum at room temperature for 3 days before use. Aqueous solutions with polymer concentrations ranging from 20% to 80% wt were prepared by mixing weighed amounts of deionized, bidistilled water with the appropriate amounts of dried HPC. The solutions were stirred daily by hand for 1 month to ensure complete dissolution. Concentrations were checked by drying under vacuum preweighed amounts of each solution and were always well within 1% of the assumed values. Polymer volume fractions v_2 were calculated by using a value of HPC density of 1.20 g/mL[16] and assuming additivity of volumes.

2.2. Optical Microscopy and Image Analysis. The VEC system used in this work is composed of a polarizing microscope (Axioscop FS, by Zeiss), a CCD B/W video camera (Hitachi, Model KPM-E1), and a frame grabber for image acquisition and processing (DT2867-LC, controlled via Global Lab Image software, by Data Translations Inc.), installed on a 80486-based host computer. The analog signal coming from the video camera is digitized by the frame grabber into an array of integers, ranging from 0 to 255, which are displayed on a monitor as gray levels. VEC optics is based on analog contrast enhancement by setting gain and offset of the incoming video signal.[28] Images were further processed to subtract camera mottle and improve contrast via software. To measure the cholesteric pitch, scale factors (μm/image pixel) were preliminarly determined by using a calibrated reticule. The optics selected for the measurements included a brightfield condenser (NA = 0.9), a 100×/1.25 Achroplan objective and an optovar slider, with magnification factors of 1.25× and 1.6× (all the components from Zeiss). The working distance of the 100× objective allowed us to focus planes inside the sample down to about 150 μm from the upper glass surface (coverslip). Such a distance can be considered deep enough to avoid surface effects. The spacing of fingerprint lines was then measured by performing the Fourier transform of the image and analyzing the resulting pattern in the frequency domain.[7] Due to the high density of defects, the fingerprint lines oriented randomly in most images and the corresponding Fourier spectrums were characterized by a bright ring, whose radius is inversely proportional to the cholesteric pitch. The rings are rather broad, leading to some uncertainty in pitch determination. The effect can be mainly attributed to deviations of the cholesteric axis from the horizontal plane or distortions in the proximity of defects, generating a local increase of the spacing of the fingerprint lines.[29] The pitch was therefore calculated from the highest value of the ring radius, corresponding to the smallest spacing in the real-space image.

Besides direct observation of cholesteric textures, the VEC system was also used to measure turbidity as a function of temperature and concentration. Within the linear range of operation of CCD camera and digitizer, the mean gray level of an image can be taken as proportional to light intensity.[28] Absorbance was therefore calculated as the ratio between the

mean gray level of an image taken inside the sample and that of a field outside (the baseline gray value, corresponding to no light hitting the camera faceplate, was preliminarily subtracted from each mean gray level). Measurements were performed with a Zeiss LD Achroplan 40×/0.6 objective either in white light or at 546 nm (by means of a green interference filter). Turbidity was then determined from the average value of absorbance over several points (5−10) within the sample. As a reference, a conventional spectrophotometer was also used to measure turbidity in samples placed in 1 cm path cuvettes.

To control the temperature, the microscope was placed in a Plexiglas box with a water-circulating radiator connected to a water bath acting as a cooling/heating element. To ensure that equilibrium conditions were reached at each temperature, heating/cooling rates were kept on the order of 0.05 °C/min. Several days were required for a full scan of the temperature range investigated (from −3 to +46 °C). Samples were placed between a microscope slide and a cover slip separated by a spacer (thickness ~1 mm) and allowed to equilibrate for at least 1 day after loading. To avoid drying, samples were sealed with vacuum grease. No significant loss of solvent was found, gravimetrically, 3 days after loading the samples.

3. Results

3.1. Room Temperature Morphology. At room temperature solutions with concentrations up to 39% wt looked isotropic. At higher concentrations ringed anisotropic spherulites were dispersed in an isotropic phase. The retardation lines inside the spherulites were arranged in patterns typical of cholesteric droplets, which have been studied in detail by Bouligand and Livolant in both low and high molecular weight liquid crystals.[30] For HPC, the ringed structure of the spherulites has been reported only for solvents where the cholesteric pitch was considered resolvable in optical microscopy (such as acetic acid[5]). By means of the VEC optics used in this work, the retardation lines in water were clearly resolved, as shown in Figure 1a, down to a spacing of about 0.3 μm.

The size of the spherulites increased with increasing concentration, until (at about 46% wt) phase inversion occurred, with the formation of isotropic droplets dispersed in a liquid crystalline phase (Figure 1b, corresponding to a 50% wt solution at 25 °C). The average diameter of the isotropic droplets was a decreasing function of concentration. The 60% wt sample was still biphasic, whereas the 70% wt solution looked fully anisotropic. The cholesteric pitch, which is equal to twice the spacing between the retardation lines, decreased with increasing concentration within the biphasic region at room temperature. The fingerprint lines, indeed, were no longer resolvable above a concentration of about 50% wt. To sum up, at room temperature the following morphologies were observed: (1) isotropic (structureless) up to about 39% wt; (2) biphasic with anisotropic droplets up to about 46% wt; (3) biphasic with isotropic inclusions up to about 65% wt; (4) fully anisotropic at higher concentrations (with cholesteric structures such as polygonal focal conics and planar configurations).

3.2. Determination of the Phase Diagram. Let us consider now how temperature affects the phase behavior starting with solutions in the biphasic region at 25 °C. In a typical run, temperature was first lowered from the room value to a few degrees Centigrade. As the temperature went down, the isotropic droplets observed in solutions such as in (3) shrunk in size until they disappeared and the sample looked fully anisotropic, displaying typical cholesteric textures. For

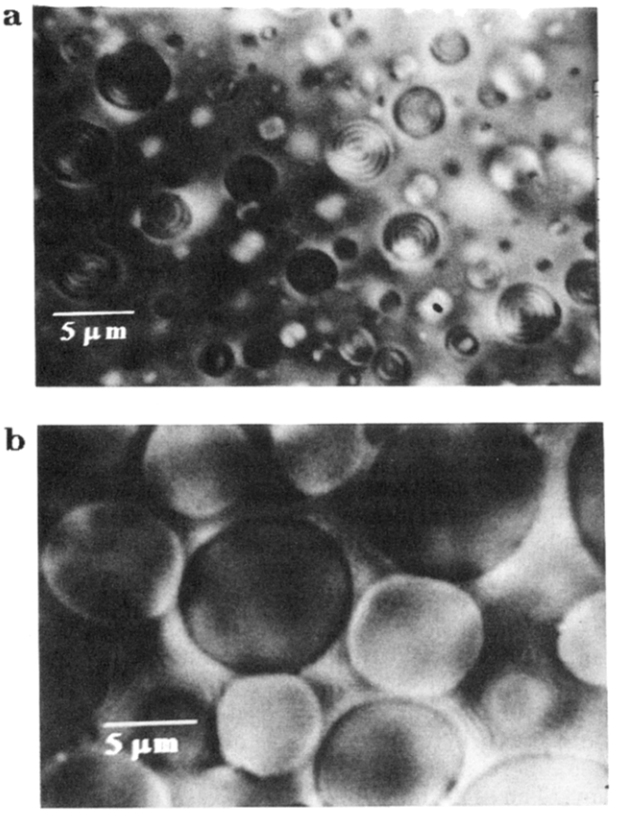

Figure 1. (a) Micrograph showing a 42% wt solution at 25 °C (crossed polars). (b) Typical morphology displayed by a 50% wt solution at 25 °C (crossed polars).

solutions such as in (2), the transition to the fully anisotropic state occurred by growth and coalescence of the anisotropic spherulites. In both cases, the temperature of the transition from the biphasic region to the fully anisotropic one increased with increasing concentration. Figure 2a shows the typical appearance of a solution in the fully liquid crystalline region (42% wt, 2 °C).

After the fully anisotropic state was reached, temperature was raised again and the point of transition to the biphasic region, as revealed by nucleation of the isotropic droplets (see Figure 2b, corresponding to a 42% wt solution at 7 °C), was noted. The transition took place at a temperature 2−5 deg higher than when cooling the sample. By further raising the temperature, the isotropic inclusions grew in size, losing their spherical shape, and nucleation of more droplets was observed in the continuous phase (Figure 2c, corresponding to a 46% wt solution at 30 °C). Two distinct morphologies were then observed, depending on concentration. For intermediate values (around 50% wt), the contour of the inclusions became irregular and the material in the continuous phase showed a higher contrast (Figure 2d, a 50% wt solution at 42 °C). At higher temperatures such morphology evolved to a gel-like network of aggregated structures in a dilute medium (Figure 2e, a 50% wt solution at 46 °C). The material was highly turbid, but light was still transmitted between crossed polars. The second morphology was observed at both higher and lower concentrations. The surface of the inclusions, which assumed a flakelike shape, became rough and irregular, but the two phases did not become interconnected, as shown in Figure 2f for a 60% wt solution at 40 °C.

Let us now turn to solutions of type (1), i.e. with concentrations below 40% wt. At room temperature,

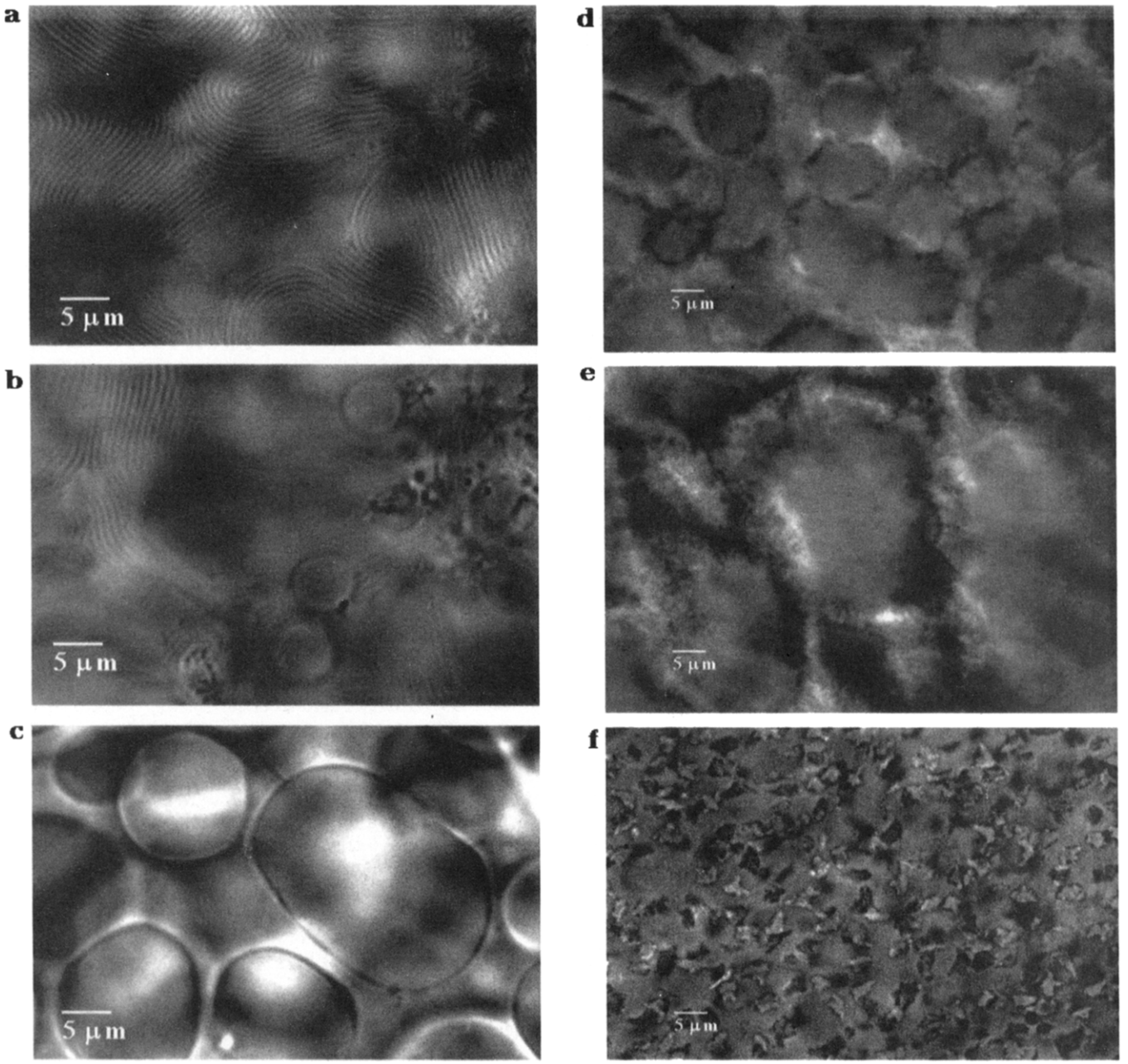

Figure 2. Sequence of micrographs showing the effect of temperature on the morphology of solutions in the wide biphasic region. Concentrations and temperatures are as follows: (a) 42% wt, 2 °C; (b) 42% wt, 7 °C; (c) 44% wt, 30 °C; (d) 50% wt, 42 °C; (e) 50% wt, 46 °C; (f) 60% wt, 40 °C.

samples in this concentration range looked isotropic. As the temperature was lowered, a new, surprising feature of the phase diagram was observed: nucleation of cholesteric droplets occurred between 30% and 39% wt, indicating that the solutions were becoming anisotropic at concentrations much below the reported limit for mesophase formation (around 40% wt). Indeed, the anisotropic phase gradually extended to the whole sample by growth and coalescence of the cholesteric droplets (see Figure 3a, for a 35% wt solution at 1 °C).

The lower the concentration, the lower was the temperature T_{i-b} at which the first appearance of the anisotropic phase was detected. At 30% wt T_{i-b} was equal to −3 °C, close to the lowest temperature allowed by the present setup. It is likely that the transition to the biphasic region may occur at even lower values of temperature and concentration, an obvious limit being posed by the transition to the solid state. When the temperature was raised again starting from the fully anisotropic phase, the point of transition to the biphasic region T_{b-a} was a few degrees higher than the one observed upon cooling the sample, as previously mentioned. Furthermore, a sharp transition from the biphasic region to the isotropic one was not observed by raising the temperature. Residual anisotropic areas enclosing isotropic droplets were still present at temperatures much above T_{i-b} and disappeared very slowly.

Another transition was observed at temperatures close to 40 °C (the exact value being a decreasing function of concentration). Spherical droplets appeared in the isotropic phase, and the sample turned white and turbid. Between crossed polars, the droplets looked anisotropic, as shown by the presence of maltese crosses (Figure 3b, for a 37% wt solution at 37 °C). Precipitating droplets were also observed in the 42% wt solution. By further increasing the temperature, the droplets became irregular in shape, with spikelike structures spread on the surface, and the maltese crosses dis-

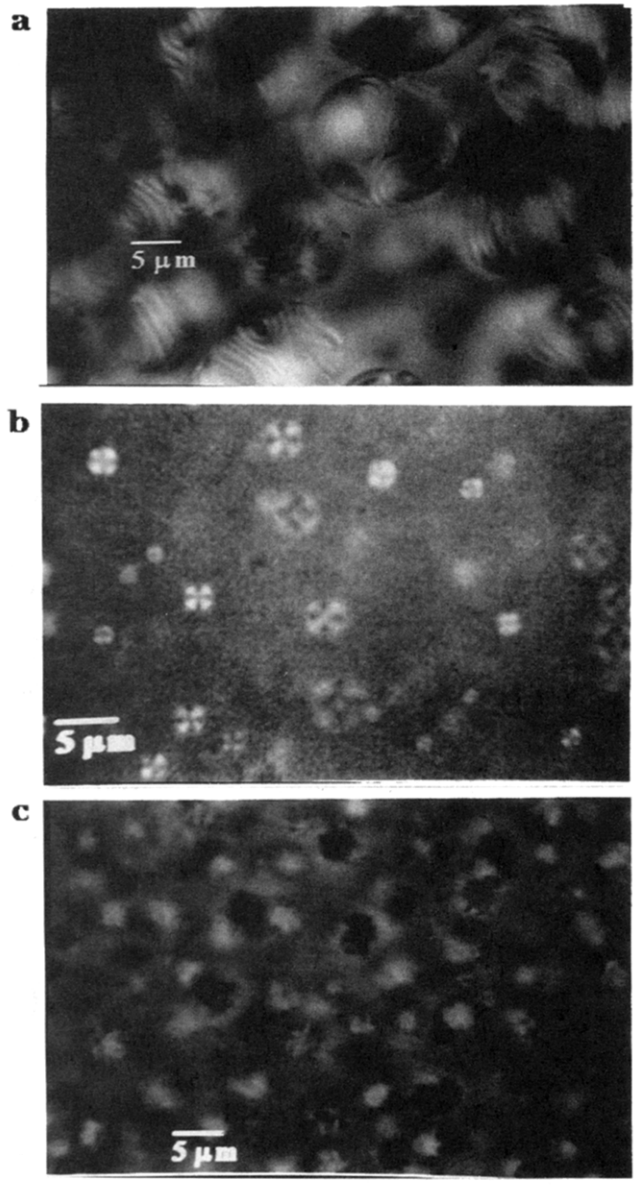

Figure 3. Sequence of micrographs showing samples with concentrations below 40% wt at different temperatures. Concentrations and temperatures are as follows: (a) 35% wt, 1 °C; (b) 37% wt, 37 °C; (c) 42% wt, 40 °C.

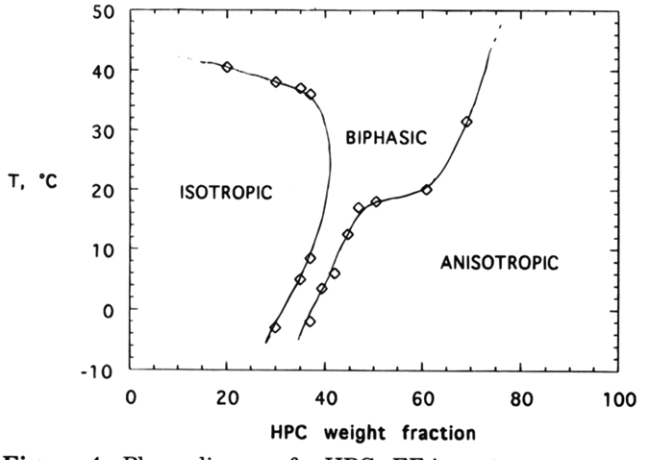

Figure 4. Phase diagram for HPC–EF in water.

appeared (Figure 3c, for a 42% wt solution at 40 °C).

These results are summarized in the phase diagram shown in Figure 4. Aside from quantitative aspects, the main novel feature with respect to the phase diagrams

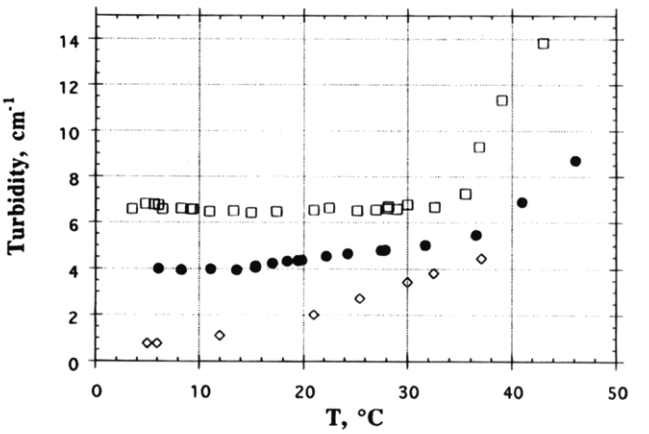

Figure 5. Turbidity vs temperature for three samples: 37% wt (squares), 50% wt (circles), and 60% wt (diamonds).

reported in the literature is the presence of a narrow biphasic region exhibiting a significant thermotropic effect. At higher temperatures the biphasic region widens up and the material resembles a gel or a precipitate, depending on concentration. The border between the isotropic and the narrow biphasic region is T_{i-b} as measured upon cooling the samples (no sharp transition was observed upon heating, as mentioned above). The temperatures T_{b-a} of transition from the biphasic region to the anisotropic one are averages of the values measured upon cooling and heating the sample, the difference being a few degrees Centigrade.

3.3. Turbidity Measurements. In Figure 5 turbidity is plotted vs temperature for three representative samples at different concentrations (37%, 50%, and 60% wt).

For the sake of clarity, the curves have been arbitrarily shifted along the turbidity axis. The curve corresponding to the 37% wt sample is representative of the trend observed in the isotropic region in Figure 4. Turbidity is constant up to the temperature corresponding to the precipitation of the anisotropic droplets, where a steep increase of absorbance is observed. The 50% wt solution displays a more complex behavior. Turbidity is constant at low temperature, where the sample is fully anisotropic, and exhibits the first gradual increase upon entering the biphasic region. Another steep increase of turbidity can be noticed at higher temperatures and is related to the appearance of the gel-like structure. For the 60% wt solution turbidity stays constant until nucleation of the first isotropic droplets takes place. A gradual, continuous increase of turbidity with temperature is then observed.

3.4. Dependence of the Helical Pitch on Concentration. The variation of the helical pitch with concentration was determined by Fourier transforming images of fingerprint lines, as described in the Experimental Section. A typical image with the corresponding Fourier transform is reported in Figure 6 (corresponding to a 37% wt solution at −3 °C).

The bright ring in the Fourier spectrum is associated with the periodicity of the randomly oriented fingerprint lines visible in the real-space image. The inverse third power of the pitch is plotted in Figure 7 as a function of the volume fraction v_2 in the range where the spacing of the fingerprint lines is resolvable in optical microscopy (up to about 50% wt). The solid line is the best fit by the least squares method to the experimental data (a good agreement, but with a lower correlation coefficient, is also obtained with an inverse second power dependence).

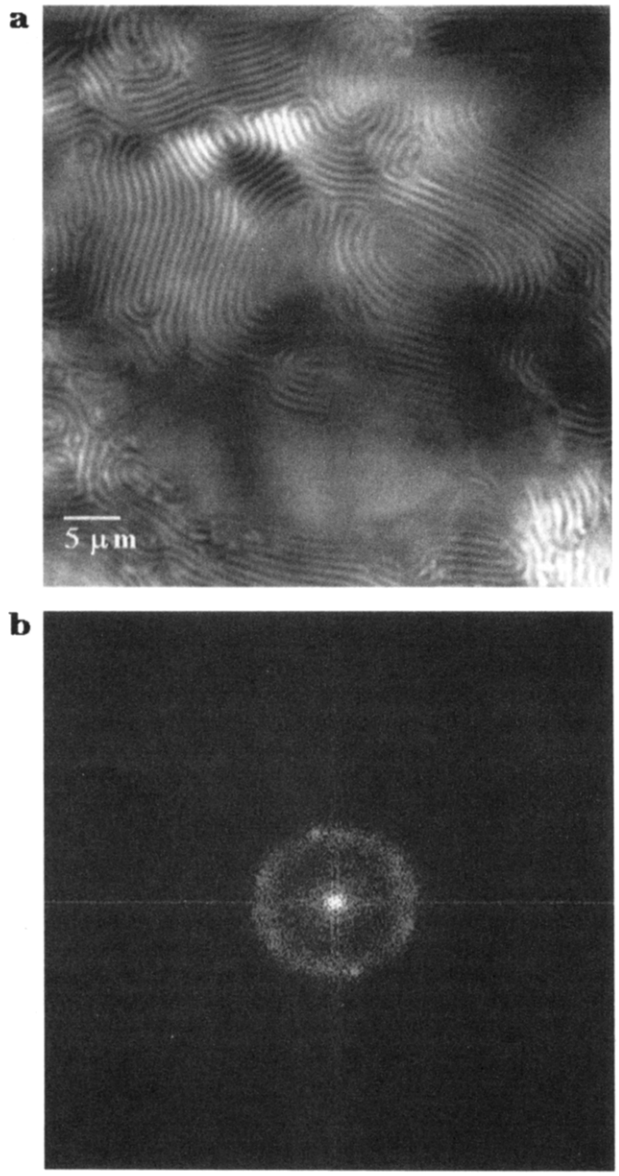

Figure 6. Micrograph of a 37% wt solution at −3 °C (a), with the corresponding Fourier transform (b).

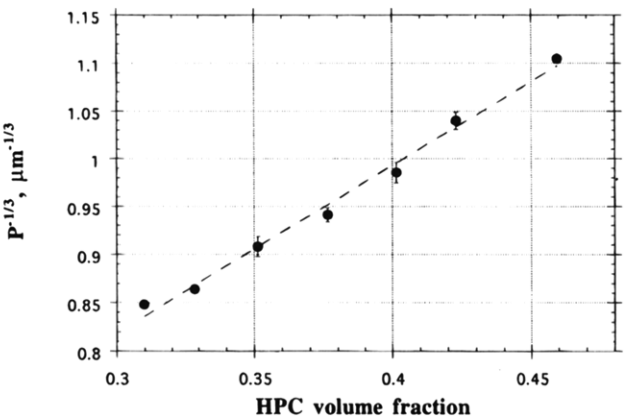

Figure 7. Plot of the inverse third power of the helical pitch as a function of HPC volume fraction.

The data in Figure 7 were taken at a temperature of 2−3°C, where the solutions were fully anisotropic, with the exception of the two points at 35% and 37% wt. At such concentrations the solutions were still biphasic at 2 °C. To study the effect of phase separation on the pitch, the variation of P with temperature was studied

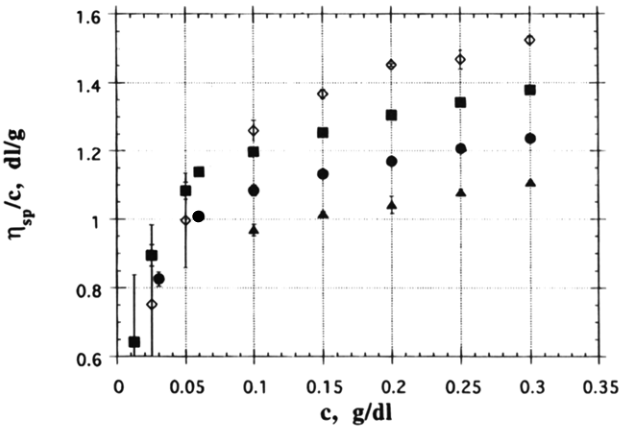

Figure 8. Plot of the specific viscosity η_{sp}/c vs concentration at the following temperatures: 1.4 °C (diamonds), 15 °C (squares), 25 °C (circles), and 35 °C (triangles).

for the 35% and 37% wt samples, starting from −2 °C (a low enough temperature to ensure that both solutions were fully anisotropic). P increased linearly with increasing temperature with a slope of about 1.6 μm/°C up to nucleation of the first isotropic droplets. From the nucleation point onward, P started decreasing with increasing concentration. Such an anomalous trend has also been observed by Fortin and Charlet[11] for solutions with concentrations above 60% wt and can be explained by phase separation. Indeed, upon entering the biphasic region two competing effects are expected: the decrease of P due to the increase of HPC concentration in the anisotropic phase and the increase of P upon heating. The observed decrease of P shows that the dependence on concentration is the prevailing effect. The values of P for the 35% and 37% wt samples in Figure 7 were obtained by extrapolating to 2 °C the values measured at temperatures below phase separation.

3.5. Intrinsic Viscosity Results. The intrinsic viscosity of HPC in water was measured in the temperature range from 1 to 35 °C. In Figure 8 the specific viscosity η_{sp}/c at several temperatures (1.4, 15, 25, and 35 °C) is plotted as a function of concentration c.

Standard deviations, shown as error bars in Figure 8, were calculated on at least four measurements of flow time at the same concentration, once steady state was reached (see Experimental Section). At each temperature, an apparent anomalous trend of η_{sp}/c was noticed; namely the curves show a downward curvature even at low c, instead of approaching a constant derivative for a vanishing concentration. Such a trend was systematic, and the values of c were not particularly low for intrinsic viscosity measurements, thus allowing one to exclude that the effect was an artifact due to experimental errors. The value of $[\eta]$ at each temperature was calculated by extrapolating the η_{sp}/c data in the linear portion of the diagram, which prevails at somewhat higher concentrations. The results are shown in Figure 9, where $\ln[\eta]$ is plotted vs temperature. Within experimental error, the data points are well represented by a linear fit (solid line) with a slope equal to about 9×10^{-3} K^{-1}.

4. Discussion

The phase diagram shown in Figure 4 differs both qualitatively and quantitatively from previous results on the thermodynamic behavior of the HPC/water system. In this section, the following issues will be discussed in some detail: (1) the temperature depen-

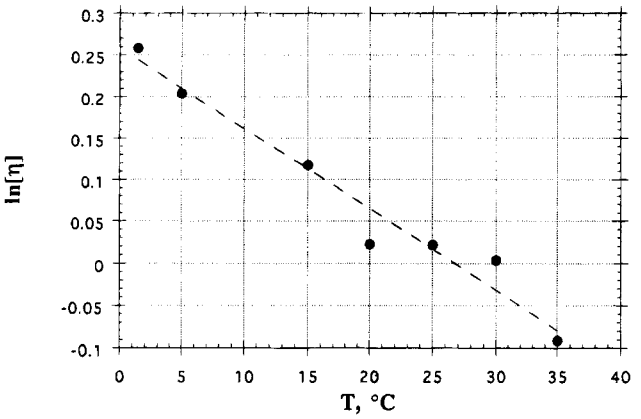

Figure 9. Plot of ln [η] as function of temperature.

dence of v'_2; (2) HPC chain flexibility; (3) polymer aggregation effects and influence of polydispersity on the phase diagram; (4) the nature of the turbid region.

4.1. Temperature Dependence of v'_2. The main qualitative difference in the phase diagram with respect to previous results for HPC in water is the marked temperature dependence of v'_2 that was found below ca. 18 °C. A similar thermotropic effect has been reported in the literature for HPC in DMAc,[9,27,31] DCA,[17,27] ethylene-based glycols,[23] dimethyl sulfoxide,[31] acetic acid,[17] trifluoroacetic acid,[23] pyridine,[6] 2-methoxyethanol,[6] and ethanol[6,17] and for other mesogenic polymers.[32] To the author's knowledge, the effect has never before been observed for HPC in water. It should be mentioned, however, that the temperature range investigated in most studies is above 20 °C.[5,9,16,18,23] A lower temperature range (starting from about 0 °C) was explored by Fortin and Charlet,[11] who measured turbidity vs temperature at several concentrations and proposed a schematic phase diagram where v'_2 and v''_2 did not depend on temperature. However, among the concentrations investigated by these authors, only one, namely 30% wt, belongs to the narrow biphasic region found in the present work. In fact, the 30% wt solution remains within the isotropic region throughout the temperature range explored by Fortin and Charlet, since, according to our estimates, T_{i-b} for the 30% wt solution falls below 0 °C.

On the basis of the assumed independence of the critical concentration on temperature, the values of v'_2 measured experimentally have so far been compared to those calculated from the athermal Flory theory for rodlike particles.[33] Satisfactory agreement has been found by using the well-known approximate equation[33]

$$v'_2 = \left(\frac{8}{x_k}\right)\left(1 - \frac{2}{x_k}\right) \qquad (2)$$

which relates the critical concentration v'_2 to the axial ratio x_k of the Kuhn segment. A less satisfactory representation of experimental data was obtained by the application of the Khokhlov–Semenov theory, as elaborated by Odijk, which is based on a wormlike chain model.[32]

The dependence of v'_2 on temperature raises two questions on the phase behavior of the HPC/water system, namely, (i) what is the physical origin of the observed thermotropic effect and (ii) how can the athermal lattice theory be used, if at all, for interpreting the experimental data in spite of the temperature dependence.

The general shape of the phase diagram in Figure 4, featuring both a wide and a narrow biphasic region, is in good agreement with predictions of the lattice theory incorporating isotropic intermolecular interactions, as represented by the familiar interaction parameter χ.[20] The significance of energetic interactions is further supported by the positive values of χ that have been obtained from gas chromatographic[34] and osmotic pressure measurements.[35] The lattice theory including isotropic energetic interactions, however, does not predict a significant dependence of v'_2 on χ (and therefore on temperature) within the narrow biphasic region.

Flory and Ronca[36] further extended the lattice theory for thermotropic LCPs by adding the contribution of soft, orientation-dependent interactions. The case where the rods are dispersed in a solvent was treated by Warner and Flory.[37] In order to assess the role of anisotropic interactions on the thermotropic effect displayed by HPC in DMAc, Conio et al.[9] calculated the phase diagram for an axial ratio of 15 according to the Warner and Flory theory.[37] The results show that only a small bending of the narrow region (toward high concentrations) is predicted by the model. A different approach was proposed by Ten Bosch et al.,[38] who derived the expression $v'_2 \sim (T/T^\circ_{NI})^2$ (where T°_{NI} is the transition temperature in the pure LCP) for wormlike chains with soft long-range interactions. Good agreement with experimental data, however, was found only for weakly polar solvents (an example is HPC in DMAc).

It so appears that soft intermolecular interactions, either isotropic or anisotropic, are insufficient to explain the observed strong temperature dependence of v'_2. However, another possible source of the thermotropic effect is chain flexibility of the HPC molecule, which has been already invoked to explain the temperature dependence of v'_2 and v''_2 in the phase diagram of HPC in DMAc.[9] HPC chain flexibility will be discussed in the following subsection.

4.2. HPC Chain Flexibility. A simple model that has been used to account for the partial rigidity of cellulose derivatives (and of HPC in particular) is the Kuhn chain, which is also readily compatible with the lattice theory.[20] The main difference with respect to the rigid rod model is that mesophase formation is governed by the axial ratio x_k of the Kuhn segment rather than by the extended length of the molecule.[20] The Kuhn segment length l_k is calculated from the mean square unperturbed end-to-end distance $\langle r_0^2 \rangle$ through the equation

$$l_k = \frac{\langle r_0^2 \rangle}{nl} \qquad (3)$$

where n is the number of repeating units in the real chain and l is the projected length of a repeating unit on the axis of the extended chain.[20] The axial ratio x_k is equal to l_k/d, where d is the chain diameter.

For cellulose derivatives, an increase of chain rigidity upon lowering the temperature has been invoked by Flory et al.[39] to explain the large negative temperature coefficients d ln η/dT (from -4.8×10^{-3} to -9.5×10^{-3} K^{-1}) of the intrinsic viscosity. The same authors proposed the following relationship

$$[\eta] = \{\Phi\}\left(\frac{\langle r_0^2 \rangle}{M}\right)^{3/2} M^{1/2}\alpha^3$$

where α is the linear expansion due to excluded volume

effects and $\{\Phi\}$ is an increasing function of molecular weight, approaching the asymptotic, universal value of 2.2×10^{21} as $M \rightarrow \infty$. For cellulose derivatives experimental values of $d\ln \alpha^3/dT$ are much smaller than (and opposite in sign to) $d\ln \eta/dT$. By neglecting the slight increase of $\{\Phi\}$ with temperature, Flory et al.[39] concluded that $d\ln \eta/dT$ is approximately representative of $d\ln (\langle r_0^2\rangle/M)^{3/2}/dT$.

The analysis outlined above suggests a relatively simple experimental way to assess the hypothesis that the v'_2 dependence on temperature is mainly due to variation of chain rigidity. From measurements of intrinsic viscosity vs temperature one can determine $d\ln \eta/dT$. From the latter quantity (being representative of $d\ln (\langle r_0^2\rangle/M)^{3/2}/dT$, as discussed above), a value of $d\ln x_k/dT$ can be estimated by using eq 3 (and by neglecting the variation of d with temperature). Now, since an independent estimate of $d\ln x_k/dT$ can be obtained from the phase diagram by determining the slope of v'_2 in the narrow biphasic region (and by using eq 2), the two values of $d\ln x_k/dT$ can be compared to assess the role of chain flexibility on the thermotropic effect. In general, the use of a Gaussian relationship for semirigid chains is not a commandable approach. However, the procedure just described is justified by the following points: (i) it is well established that excluded volume effects are negligible for cellulosic chains, as mentioned before; (ii) the procedure is only based on a comparison of slopes.

Such procedure can be applied to results already available in the literature for HPC in DMAc. Values of $d\ln \eta/dT$ varying from -9.7×10^{-3} to -6.7×10^{-3} K^{-1} have been reported by Korneeva et al.[26] for HPC fractions in DMAc and in TChE. From these data, an estimate of $d\ln x_k/dT$ equal to -6.4×10^{-3} K^{-1} can be calculated for HPC in DMAc. Good agreement is found with values of $d\ln x_k/dT$ inferred from the phase diagrams reported by several authors for HPC in DMAc[17,23,27,31] (such values are in the range $5 \times 10^{-3} - 6 \times 10^{-3}$ K^{-1}).

For HPC in water, $d\ln x_k/dT$ of the order of 1.5×10^{-2} K^{-1} can be determined from the phase diagram shown in Figure 4 and is in reasonable agreement with the value of 9×10^{-3} K^{-1} that can be inferred from Figure 9, taking into account the procedure used to calculate $[\eta]$. A value of $d\ln x_k/dT$ much closer to 9×10^{-3} K^{-1} is obtained by taking into account the effect of anisotropic soft interactions (the temperature T^* representative of the intensity of soft interactions was taken equal to 75 K, the value reported by Conio et al.[9] for HPC in DMAc). The discrepancy might also reflect a change of the average size of HPC aggregates as a function of temperature (see next subsection).

Having recognized chain flexibility as a good candidate to explain the thermotropic effect, it can be concluded that the Flory–Ronca theory gives the best agreement with the available data, provided that the dependence of the axial ratio on temperature is taken into account. However, a full test of the validity of the theory for the HPC/water system would require the knowledge of the axial ratio at several temperatures. For HPC in water, such data are not available in the literature. On a molecular basis, chain rigidity is associated with strong hydrogen bonding, both intramolecular and with water molecules. The role of water structuring by hydrogen bonds, which is dependent on temperature and concentration, has been pointed out by Fortin and Charlet.[11]

4.3. Polymer Aggregation Effects and Influence of Polydispersity on the Phase Diagram. The anomalous trend of η_{sp}/c vs c pointed out in the Results can be explained by the presence of small polymeric aggregates, which tend to dissociate at low concentration and low temperature. The increase of solubility with decreasing temperature for HPC in water[25] is in line with this interpretation. Direct evidence for the presence of small polymeric aggregates, even at low concentration, has been provided by Winnik et al.[24,40] by fluorescence spectroscopy. Polymer aggregation has been invoked by Werbowyj and Gray[16] to explain an apparent increase with time of M_w measured by light scattering.

Considering now the effect of polydispersity, a relevant quantity for comparison with theory is the ratio of the limiting concentrations in the narrow biphasic region, v''_2/v'_2. From the phase diagram of Figure 4 a value of about 1.2 is obtained for v''_2/v'_2, which is on the same order of magnitude of literature data (1.2 for HPC in water and DMAc,[9] 1.29–1.37 in four different solvents[17]). These results are close to the predictions of the Flory theory for monodisperse rods ($v''_2/v'_2 = 1.367$ for an axial ratio equal to 20), in spite of the broad distribution of molecular weights reported for commercial HPC samples.[1]

However, several experimental results are at variance with the Flory theory for monodisperse rods. Indeed, Conio et al.[9] found that the concentrations of the phases coexisting at a given temperature are a function of the average concentration v_2 of the system, instead of remaining constant, as predicted by the theory for monodisperse rods. Furthermore, a significant fractionation effect was observed, with an enrichment of high molecular weights in the anisotropic phase. The same authors, however, raised some questions about the validity of their own results, which could be significantly biased by large nonequilibrium effects associated with the separation process by ultracentrifugation.

Such complications can be avoided by means of the VEC microscopy technique used here, which allows one to observe *in situ* the effects of polydispersity. Indeed, in the biphasic region the change of the concentration of the anisotropic phase with v_2 can be revealed by the variation of the helical pitch P with v_2. We observed, in fact, such an effect in a qualitative way. A quantitative measurement of the effect was not made, however, for two good reasons. On the one hand, at some point in the range of composition corresponding to the biphasic region the spacing between retardation lines becomes unresolvable. Furthermore, even for the values of v_2 where the pitch is resolvable, a precise determination of the concentration of the anisotropic phase from the value of P is hampered by the fact that, at a given concentration and temperature, P is also expected to be a function of molecular weight[8] (though, for HPC in water in particular, the M_w dependence is not strong[3]).

Another experimental result which is at variance with the theory for Kuhn chains is the fractionation of molecular weights between the coexisting phases.[9] The effect takes place on time scales longer than phase separation, since partitioning of components between phases occurs through diffusive transport, a much slower process than orientational ordering of the molecules.[20] In this work, an example of such a slow equilibration process was found in the persistence of residual anisotropic areas upon raising the temperature above T_{i-a}. Within the biphasic region, the occurrence

of fractionation could also be revealed by a variation of P with time (at a given concentration), as long as the pitch is a function of molecular weight. No appreciable change of P with time was observed in this work, thus confirming the weak dependence of P on M_w for HPC in water.

4.4. Nature of the Turbid Region. Finally, let us consider the phase behavior in the biphasic region at temperatures above the transition to a turbid appearance. As shown by the micrographs of Figures 2e,f, and 3b, the morphology depends on sample concentration. At both very low and very high concentrations, spherical structures are found (anisotropic and isotropic, respectively), which are dispersed in a continuous medium. The observation of anisotropic droplets precipitating from dilute solutions (Figure 3b) can be related to the circular reflectivity spectra measured by Fortin and Charlet,[11] showing that the concentrated phase formed upon heating dilute solutions exhibits cholesteric order. Such a result would be in agreement with the spherulite-like structure here observed if the dark cross inside the spherulite is interpreted as due to cholesteric order, the fingerprint spiral pattern inside the spherulite not being resolvable because of the high polymer concentration. The knowledge of the structure of the spherulites is essential to ascertain the nature of the heat-induced phase separation, which is still an open issue. The problem has been recently addressed in a paper by Larez et al.,[41] according to which phase separation is driven by the formation of a mesophase upon entry into the wide region (eventually followed by crystallization).

A different morphology is observed at intermediate concentrations, i.e. a three-dimensional network structure (a requisite to qualify the phase as a gel). Images of the network close to the coverslip show the presence of ordered structures in the polymer-rich phase, suggesting the occurrence of crystallization (a phenomenon sometimes associated with gelation[32]). The surprising result of a concurrent existence of a gel and a liquid crystalline order has been found already in chitin solutions, as pointed out by Ciferri.[32] At intermediate concentrations, the evolution of solutions upon heating (see Figure 2) suggests liquid–liquid phase separation as a possible mechanism of gel formation. Indeed, the growth in size of isotropic droplets upon heating is associated with a corresponding increase in concentration of the anisotropic phase, which looks darker under the microscope (see Figure 2). Such a mechanism is in agreement with the light scattering results by Kyu et al.,[18,22,42] showing that phase separation begins by spinodal decomposition. More work is in progress to further elucidate the structural properties of HPC solutions in the turbid state.

5. Conclusions

The conclusions that can be drawn from this work concern the specific system investigated, i.e. HPC in water, and, more in general, the adopted methodology, i.e. VEC microscopy. As regards the first aspect, the main results are (i) the strong thermotropic effect found in the low-temperature range explored (below ca. 18 °C), (ii) the evidence for phase separation at concentrations as high as 60% wt at room temperature (showing that the biphasic region is significantly wider than previously reported), (iii) the negative temperature coefficient of the intrinsic viscosity, and (iv) the different morphologies observed in the turbid state as a function of concentration.

The thermotropic effect is relevant for the application of HPC in water as a model system in the field of LCP rheology. Indeed, in order to avoid complications due to phase separation, rheological experiments should be carried out either at concentrations larger than usually adopted or below room temperature. Furthermore, the evidence of an increase of chain flexibility with temperature, provided by the negative temperature coefficient of the intrinsic viscosity, shows that HPC in water is far from being a rigid molecule. While this result makes HPC in water a better model system for the thermotropic LCPs of industrial relevance, care should be exercised when comparing rheological results to theoretical predictions, strictly based on the rigid rod model.[43] As regards the morphologies in the turbid state, this study shows that the gel-like structure so often referred to is, in fact, present only at intermediate concentrations, whereas interconnectivity is lost at both lower and higher values of v_2.

A more general conclusion concerns the application of VEC microscopy as a tool to investigate the phase behavior of LCP solutions. The video enhancement of contrast allows one to fully exploit the resolving power of the light microscope, thus enabling the visualization of features, such as the fingerprint texture, which have been considered before as unresolvable for the HPC/water system. Furthermore, the possibility of optically sectioning the sample at high magnification allows one to examine highly turbid materials, while a scattering pattern can be also derived by Fourier transforming the real-space image.[44] It so appears that VEC microscopy can usefully be added to the other techniques usually employed to investigate polymeric materials.

Acknowledgment. This work has been supported by the Italian Ministry for University and Research (MURST) within a project on liquid crystalline polymers coordinated by Prof. G. Marrucci, whose constant encouragement and advice is gratefully acknowledged.

References and Notes

(1) Wirick, M. G.; Waldman, M. H. *J. Appl. Polym. Sci.* **1970**, *14*, 579.
(2) Werbowyj, R. S.; Gray, D. G. *Mol. Cryst. Liq. Cryst.* **1976**, *34*, 97.
(3) Werbowyj, R. S.; Gray, D. G. *Macromolecules* **1984**, *17*, 1512.
(4) Robinson, C. *Trans. Faraday Soc.* **1956**, *52*, 571.
(5) Fried, F.; Sixou, P. *J. Polym. Sci., Polym. Chem. Ed.* **1984**, *22*, 239.
(6) Tsutsui, T.; Tanaka, R. *Polym. J.* **1980**, *12*, 473.
(7) Guido, S. *Mol. Cryst. Liq. Cryst., in press.*
(8) Uematsu, I.; Uematsu, Y. *Adv. Polym. Sci.* **1984**, *59*, 37.
(9) Conio, G.; Bianchi, E.; Ciferri, A.; Tealdi, A.; Aden, M. A. *Macromolecules* **1983**, *16*, 1264.
(10) Dayan, S.; Fried, F.; Gilli, J. M.; Sixou, P. *J. Appl. Polym. Sci., Appl. Polym. Symp.* **1983**, *37*, 193.
(11) Fortin, S.; Charlet, G. *Macromolecules* **1989**, *22*, 2286.
(12) Keates, P.; Mitchell, G. R.; Peuvrel, E. *Polymer* **1992**, *33*, 3298.
(13) Navard, P.; Haudin, J. M.; Dayan, S.; Sixou, P. *J. Appl. Polym. Sci., Appl. Polym. Symp.* **1983**, *37*, 211.
(14) Onogi, Y.; White, J. L.; Fellers, J. F. *J. Polym. Sci., Polym. Phys. Ed.* **1980**, *18*, 663.
(15) Spontak, R. J.; El-Nokaly, M. A.; Bartolo, R. G.; Burns, J. L. In *Polymer Solutions, Blends, and Interfaces*; Noda, I., Rubingh, D. N., Eds.; Elsevier: New York, 1992; p 273.
(16) Werbowyj, R. S.; Gray, D. G. *Macromolecules* **1980**, *13*, 69.
(17) Bheda, J.; Fellers, J. F.; White, J. L. *Colloid Polym. Sci.* **1980**, *258*, 1335.
(18) Kyu, T.; Mukherjee, P. *Liq. Cryst.* **1988**, *3*, 631.
(19) Suto, S.; Kimura, S.; Karasawa, M. *J. Appl. Polym. Sci.* **1987**, *33*, 3019.
(20) Flory, P. J. *Adv. Polym. Sci.* **1984**, *59*, 1.
(21) Guido, S.; Grizzuti, N. *Rheol. Acta* in press.

(22) Mukherjee, P.; Kyu, T. *Polym. Prepr. (Am. Chem. Soc., Div. Polym. Chem.)* **1987**, *28*, 361.
(23) Seurin, M. J.; Gilli, J. M.; Fried, F.; Bosch, A. T.; Sixou, P., in *Polymeric Liquid Crystals*; Blumstein, A., Ed.; Plenum: New York, 1985; p 377.
(24) Winnik, F. M. *Macromolecules* **1987**, *20*, 2745.
(25) Klug, E. D. *J. Polym. Sci., Part C* **1971**, *36*, 491.
(26) Korneeva, E. V.; Shtennikova, I. N.; Shibaev, V. P.; Klenin, S. I.; Kolbina, G. F.; Ekaeva, I. V.; Didenko, S. A. *Eur. Polym. J.* **1990**, *26*, 781.
(27) Aden, M. A.; Bianchi, E.; Ciferri, A.; Conio, G.; Tealdi, A. *Macromolecules* **1984**, *17*, 2010.
(28) Inoué, S. *Video Microscopy*; Plenum Press: New York, 1986.
(29) Livolant, F. *J. Phys. (Paris)* **1986**, *47*, 1605.
(30) Bouligand, Y.; Livolant, F. *J. Phys.* **1984**, *45*, 1899.
(31) Suto, S.; Obara, K.; Nishitani, S.; Karasawa, M. *J. Polym. Sci., Part B: Polym. Phys.* **1986**, *24*, 1849.
(32) Ciferri, A., In *Liquid Crystallinity in Polymers*; Ciferri, A., Ed.; VCH Publishers, Inc.: New York, 1991; p 209.
(33) Flory, P. J. *Proc. R. Soc. London, Ser. A* **1956**, *234*, 73.
(34) Aspler, J. S.; Gray, D. G. *Macromolecules* **1979**, *12*, 562.
(35) Bergman, R.; Sundelöf, L.-O. *Eur. Polym. J.* **1977**, *13*, 881.
(36) Flory, P. J.; Ronca, G. *Mol. Cryst. Liq. Cryst.* **1979**, *54*, 311.
(37) Warner, M.; Flory, P. J. *J. Chem. Phys.* **1980**, *73*, 6327.
(38) Bosch, A. T.; Maissa, P.; Sixou, P. In *Polymeric Liquid Crystals*; Blumstein, A., Ed.; Plenum: New York, 1985; p 109.
(39) Flory, P. J.; Spurr, K.; Carpenter, D. K. *J. Polym. Sci.* **1958**, *27*, 231.
(40) Winnik, F. M.; Winnik, M. A.; Tazuke, S.; Ober, C. K. *Macromolecules* **1987**, *20*, 38.
(41) Larez-V, C.; Crescenzi, V.; Ciferri, A. *Macromolecules* in press.
(42) Kyu, T.; Zhuang, P.; Mukherjee, P. *J. Appl. Crystallogr.* **1988**, *21*, 828.
(43) Marrucci, G.; Greco, F. *Adv. Chem. Phys.* **1993**, *58*, 331.
(44) Chowdhury, A. H.; Russo, P. S. *J. Chem. Phys.* **1990**, *92*, 5744.

MA950086U